The Journal of Experimental Biology 213, 3769-3777

doi:10.1242/jeb.046946

Sensing the strike of a predator fish depends on the specific gravity of a prey fish

William J. Stewart* and Matthew J. McHenry

Department of Ecology and Evolution, 321 Steinhaus Hall, University of California, Irvine, CA 92697-2525, USA

*Author for correspondence (wstewart@uci.edu)

Accepted 23 August 2010

SUMMARY

The ability of a predator fish to capture a prey fish depends on the hydrodynamics of the prey and its behavioral response to the predator's strike. Despite the importance of this predator–prey interaction to the ecology and evolution of a diversity of fish, it is unclear what factors dictate a fish's ability to evade capture. The present study evaluated how the specific gravity of a prey fish's body affects the kinematics of prey capture and the signals detected by the lateral line system of the prey during the strike of a suction-feeding predator. The specific gravity of zebrafish (*Danio rerio*) larvae was measured with high precision from recordings of terminal velocity in solutions of varying density. This novel method found that specific gravity decreased by ~5% (from 1.063, *N*=8, to 1.011, *N*=35) when the swim bladder inflates. To examine the functional consequences of this change, we developed a mathematical model of the hydrodynamics of prey in the flow field created by a suction-feeding predator. This model found that the observed decrease in specific gravity due to swim bladder inflation causes an 80% reduction of the flow velocity around the prey's body. Therefore, swim bladder inflation causes a substantial reduction in the flow signal that may be sensed by the lateral line system to evade capture. These findings demonstrate that the ability of a prey fish to sense a predator depends crucially on the specific gravity of the prey.

Key words: lateral line system, hair cells, predator–prey interaction, density, specific gravity.

INTRODUCTION

A broad diversity of fish prey on smaller fish using suction feeding (Lauder, 1980; Ferry-Graham and Lauder, 2001; Juanes et al., 2002). The flow created by a feeding strike can be detected by the lateral line system of the prey to trigger an evasive escape response (Eaton et al., 1977; McHenry et al., 2009). Therefore, the success of a predator's strike depends on hydrodynamics, which determine the speed of capture and the flow stimulus that alerts the prey. Although the hydrodynamics of suction feeding have been well explored (Muller et al., 1982; Lauder and Clark, 1984; Van Leeuwen and Muller, 1984), the mechanics of prey capture are only a recent area of investigation (Wainwright and Day, 2007; Skorczewski et al., 2010) and it remains unclear as to what factors determine the mechanical signals detected by a prey fish. Understanding these dynamics has the potential to reveal major factors that mediate the evolution of this predator–prey interaction.

Suction feeding is accomplished by the rapid expansion of a predator's buccal cavity and jaws. Buccal expansion creates low pressure, which drives water flow towards the predator's mouth. Prey are most commonly targeted in the region directly in front of the predator (Holzman et al., 2007; Holzman and Wainwright, 2009), where the flow field is laminar and may be approximated by a pressure gradient (Muller et al., 1982; Wainwright et al., 2007; Wainwright and Day, 2007) with increasing velocity toward the mouth (Fig. 1). The gradient generates lower pressure on the surfaces of the prey's body closer to the mouth, which creates a pressure gradient force that dominates the hydrodynamics of prey capture (Wainwright and Day, 2007). The pressure gradient force is proportional to the volume of the body and accelerates the prey at a rate that is inversely proportional to its density. Therefore, the kinematics of prey capture may be predicted from a description of the flow and pressure field created by the predator and measurements of the volume and density of the prey's body.

The dynamics of prey capture largely determines the signals detected by the lateral line system of the prey. In larval fish, this system includes a single type of hydrodynamic receptor, the superficial neuromast, which extends from the surface of the body into the water (Fig. 1). Superficial neuromasts are sensitive to fluid shearing, which is created by a difference in velocity between the body and the water (Windsor and McHenry, 2009). In the pressure gradient generated by suction feeding, this relative flow velocity is created by a difference in density between the body and the water. The ratio of body to water density, equal to the specific gravity, must deviate from unity to create a signal that may be detected by the lateral line system (Fig. 1B,C). Therefore, variation in specific gravity has the potential to affect both the rate at which a larval prey is captured and the signal detected by the lateral line system. The aims of the present study were to measure the specific gravity of the body of zebrafish (*Danio rerio*) larvae and to relate these measurements to prey capture hydrodynamics and lateral line function using mathematical modeling.

The specific gravity of a larva's body was anticipated to change within the first week of growth owing to swim bladder inflation. In zebrafish, swim bladder inflation occurs within 2 days of hatching [by 4 days post-fertilization (dpf)], when larvae begin to actively forage (Robertson et al., 2007; Lindsey et al., 2010). The swim bladder fills to ~5% of body volume with oxygen-rich gas that has a density that is 1000 times less than the surrounding tissue (Scholander et al., 1951; Alexander, 1966; Robertson et al., 2008; Lindsey et al., 2010). This event presents a potentially rapid change in specific gravity with unclear implications for prey capture.

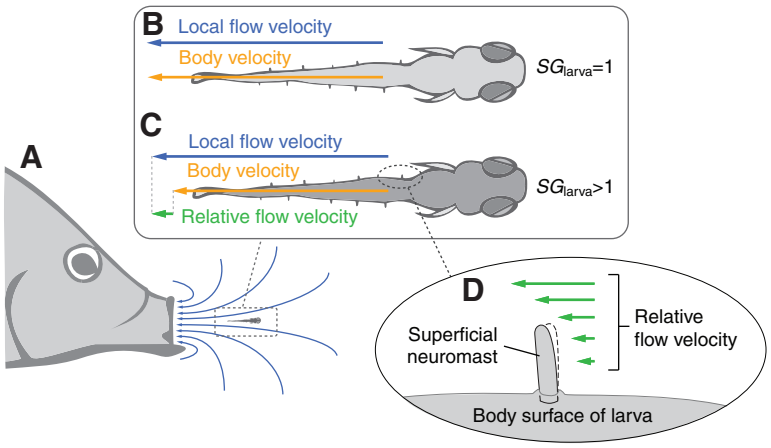

Fig. 1. A suction-feeding predator creates a sensory signal for a prey fish. (A) The predator feeds by expanding its buccal cavity to draw water and the prey towards the mouth. (B,C) The fluid velocity experienced by the prey (relative flow velocity, green) is the difference in velocity between the flow (blue) and prey's body (orange). (B) A prey fish having a specific gravity (*SG*) of unity will accelerate at the same rate as the surrounding water and therefore generates no relative velocity. (C) A larva with *SG*>1 encounters a relative flow velocity (green arrow) directed toward the predator's mouth. (D) The relative flow velocity creates fluid shearing at the body surface. Larval prey are capable of responding to this signal with an evasive escape response.

MATERIALS AND METHODS

Animals

Zebrafish larvae were raised using standard culturing techniques. A breeding colony of wild-type (AB line) zebrafish (*Danio rerio*, Hamilton 1922) was housed in a flow-through tank system (Aquatic Habitats, Apopka, FL, USA) that was maintained at 28.5°C on a 14 h:10 h light:dark cycle. The fertilized eggs from randomized mating were cultured according to standard protocols (Westerfield, 1993) and larvae were raised in an incubator in embryo medium buffered with Tris (Brand et al., 2002), from which 43 individuals (*N*=12 at 3 dpf, *N*=10 at 4 dpf, *N*=11 at 5 dpf, and *N*=10 at 6 dpf) were randomly selected for experimentation.

Body density measurements

The body density of anesthetized larvae was calculated from measurements of their terminal velocity as they passively sank or ascended through solutions of varying density (Fig. 2A,B). This novel method of measuring body density was developed to improve on the precision of density gradient methods (Coombs, 1981; Stenevik et al., 2008; Lindsey et al., 2010) and to avoid exposing larvae to solutions that could alter the tissue density through osmosis. Although density gradient methods have revealed that large-scale changes in body density occur throughout ontogeny in zebrafish (see Lindsey et al., 2010), the present study investigated subtle density changes over a much shorter period of growth (3–6 dpf), which necessitated the improved precision of the current method. For this technique, we built a series of 16 chambers (chamber dimensions: 75×25×25 mm, height × width × length) made of clear acrylic. Each chamber contained a solution with a density that was controlled by the addition of heavy water (a 99% solution of deuterium oxide, D_2O, with a density of 1.105 g ml^{-1}; Sigma-Aldrich, St Louis, MO, USA) to embryo medium buffered with Tris (Westerfield, 1993). Although pure D_2O is ~11% denser than H_2O, it does not appear to affect the osmotic balance of a larva's body with the surrounding solution. Solutions of varying heavy water concentration were created with density ranging from 0.998 to 1.070 g ml^{-1}. Solution density was measured by weighing a filled 25 ml volumetric flask on a high-precision scale (model A-200DS; Denver Instrument, Bohemia, NY, USA). Density changes created by the evaporation of hygroscopic heavy water were minimized by sealing the chamber. Furthermore, we found that solutions exposed to ambient air for 12 h exhibited very small (<0.0001 g ml^{-1}) changes in fluid density, which suggests that brief (<1 min) openings of the chamber during experiments caused negligible change.

The vertical movement of a larva within an experimental chamber was measured from video recordings (Fig. 2A,B). A video camera (Marlin, 640×480 pixel resolution, 30 frames s^{-1}; Allied Vision Technologies, Stradtora, Germany) equipped with a macro lens (50 mm, model 5023973; Sigma, Ronkonkoma, NY, USA) recorded a larva in a single chamber (field of view, 3×2.25 cm, width × height). Between recordings, the chambers were translated on a sliding base to position a new chamber into the camera's field of view. Before experiments, each larva was anesthetized in a solution of 0.0017 g l^{-1} tricaine methanesulfonate (MS-222; Finquel, Argent Chemical Laboratories, Redmond, WA, USA) and embryo medium buffered with Tris (pH ~7) to prevent active swimming during trials. A random number generator determined the chamber sequence in which terminal velocity trials were conducted for each larva.

Larvae were transferred carefully between chambers during experiments to minimize convection within a chamber and mixing between solutions. Each larva was transferred between chambers by pipette through three washes, each containing the identical solution mixture to that of the next chamber. After pipetting the larva into the new chamber, its position was carefully manipulated into the center of the chamber with a 100 µm tungsten wire before taking a displacement recording. We restarted trials if a larva exhibited significant lateral displacement, was positioned within 10 mm of a chamber wall or was displaced by probe movement. After completion of a trial (<1 min), the larva was transferred back to the MS-222 solution for 5 min before proceeding to the next measurement. Once experiments were complete, any larva exhibiting poor blood circulation or visible lacerations under a microscope (AxioCam HRc camera; Carl Zeiss, Thornwood, NY, USA) was eliminated from the study. This procedure was repeated for all 43 larvae included in the study.

The position of a larva was digitally tracked to determine the terminal velocity in each chamber (Fig. 2B). For each recording, the eyes provided discrete dark landmarks that were tracked by custom image-processing software (written in Matlab, v. 2009a; MathWorks, Natick, MA, USA). We modeled the hydrodynamics of the larval body in free fall to precisely determine the terminal velocity from our recordings of body position (Fig. 2C,D). This model assumed that the product of body mass and acceleration is equal to the sum of body weight, buoyancy and viscous drag. This differential equation may be solved analytically for velocity (U_{body}) by assuming a zero initial velocity to yield the following relationship:

$$U_{body} = U_{term}(1 - e^{-t/\tau}), \quad (1)$$

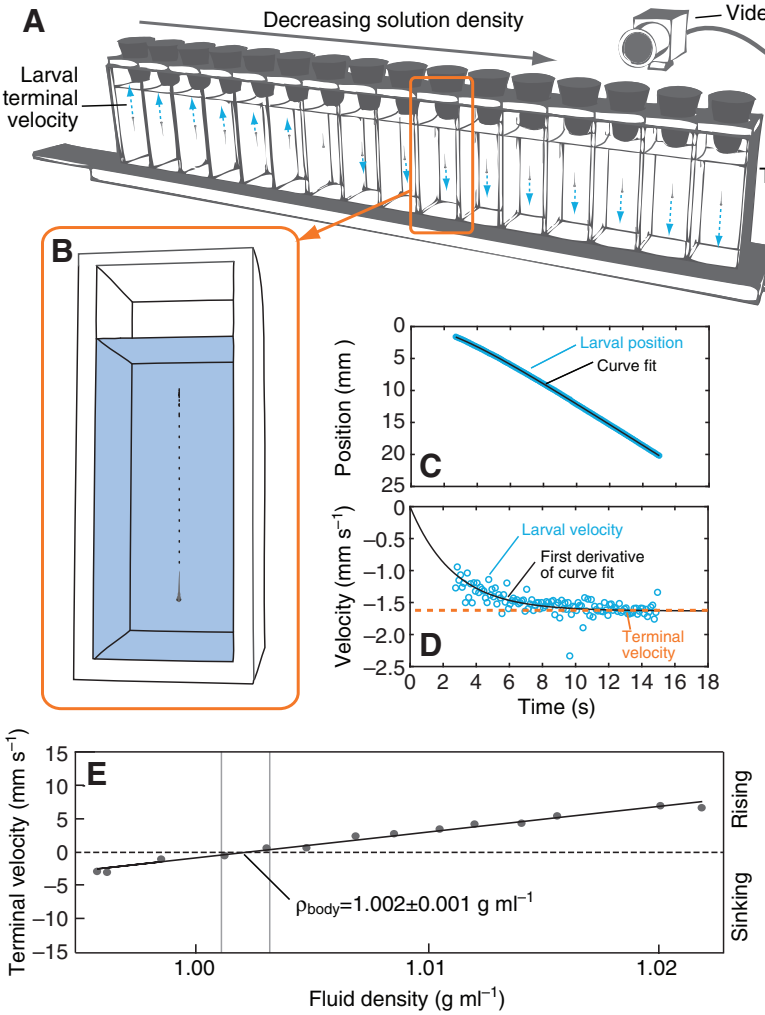

Fig. 2. Measurement of body density from terminal velocity recordings. (A) Schematic of the custom 16-chamber system used for estimating terminal velocities of anesthetized zebrafish larvae in solutions of different density. Solution density decreases from 1.070 g ml^{-1} in the left-most chamber to 0.998 g ml^{-1} in the right-most chamber. Blue arrows represent the directions and approximate magnitude of the terminal velocity achieved by a larva in each solution. (B) A single chamber containing a sinking, anesthetized larva, with points that approximate position over time. (C) Measurements of the position of the larva as a function of time for a single trial (blue) are shown with a nonlinear least-squares curve fit of Eqn 2 (black line), which provided a measure of terminal velocity. (D) The velocity of the body calculated from position measurements (blue circles) and from the curve fit in C (using Eqn 1, black line) that approaches the terminal velocity (orange dashed line) with time. (E) Terminal velocity achieved by a representative larva plotted as a function of fluid density. Body density (ρbody) was calculated as the *x*-intercept solution of the linear curve fit with 95% confidence intervals (vertical lines).

where U_{term} is the terminal velocity, t is time and τ is a time constant. The position of the body (Y_{body}) may similarly be solved by assuming a zero initial position:

$$Y_{body} = U_{term}[t + \tau(e^{-t/\tau} - 1)] . \quad (2)$$

For each recording of the position of a larva in free fall, U_{term} and τ were determined with a non-linear least-squares curve fit of this equation in Matlab.

We determined the body density of a larva from the relationship between solution density and terminal velocity (Fig. 2E). This relationship was well approximated by a linear least-squares curve fit. Because a zero velocity occurs when the body density (ρ_{body}) is equal to the solution, the *x*-intercept indicates the density of the body. Uncertainty in this calculation was measured with 95% confidence intervals of the *x*-intercept. The specific gravity of a larva was calculated by dividing ρ_{body} by the density of water (ρ_{water}=0.998 g ml^{-1}). All calculations were performed in Matlab.

Morphometrics

To determine how the specific gravity of the body was affected by changes in the volume of the body and swim bladder, we measured their three-dimensional shape from high-resolution photographs. A stereomicroscope (Zeiss Discovery V.20 and an AxioCam HRc camera; Carl Zeiss) was used to capture high-resolution images (1388×1040 pixels) of each larva from the lateral and dorsal perspectives (Fig. 3A,B). The shape of the body (Fig. 3C) was approximated by a series of transverse elliptical sections with major and minor axes equal to half the body measurements of width and height (McHenry and Lauder, 2006). From these measurements, we calculated the volume of the body (V_{body}) by integrating the area of elliptical sections ($\pi a_i b_i$, where a_i and b_i are the axes of the elliptical section in the dorso-ventral and medio-lateral directions, respectively) along the length of the body:

$$V_{body} = \pi \sum_{i=1}^{n} a_i b_i \, \Delta y , \quad (3)$$

where n is the number of elliptical sections along the rostro-caudal body axis and y is the rostro-caudal length of each section. These and all other numerical integrations were performed in Matlab using the trapezoidal method. The volume of the swim bladder (V_{SB}) was approximated using the following equation for the volume of an ellipsoid:

$$V_{SB} = \frac{4}{3}\pi ABC , \quad (4)$$

where A, B and C are the elliptical axes of the swim bladder in the medio-lateral, horizontal (s) and vertical (q) dimensions, respectively (Fig. 3C). These were measured from high-magnification photographs of the swim bladder (1.3×1.0 mm field of view) from the dorsal and lateral perspectives. The mass of the body (M_{body}) and mass of the swim bladder (M_{SB}) were calculated as the product of their respective density (from terminal velocity measurements)

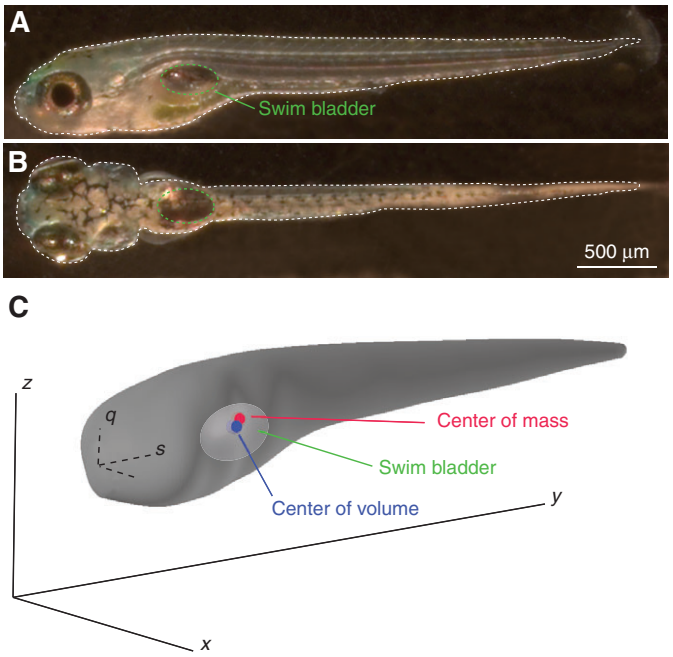

Fig. 3. Three-dimensional reconstruction of the body shape of a larva. The peripheral shape of the body and swim bladder was traced from photographs of a larva from (A) lateral and (B) dorsal perspectives. (C) By approximating the transverse shape of these morphologies as a series of ellipses, the larva's body was constructed in three dimensions. The coordinates for the earthbound frame of reference (x, y, z) and the larval frame of reference (s, q) are included. From this reconstruction and our measurements of tissue density (Fig. 1), we calculated the centers of mass and volume for the body (see Materials and methods for details).

and volume ($M_{body}=\rho_{body}V_{body}$ and $M_{SB}=\rho_{SB}V_{SB}$, where $\rho_{SB}=1.31\,mg\,cm^{-3}$) and the mass of the tissue (M_{tissue}) was calculated as the difference between these values ($M_{tissue}=M_{body}-M_{SB}$). The volume of tissue (V_{tissue}) in the body was calculated as the difference between the body volume (V_{body}) and swim bladder volume (V_{SB}) ($V_{tissue}=V_{body}-V_{SB}$) and the tissue density (ρ_{tissue}) was subsequently calculated ($\rho_{tissue}=M_{tissue}/V_{tissue}$).

We considered how swim bladder inflation influenced the distribution of mass in the body by measuring the centers of volume (COV) and mass (COM) and the moment of inertia (I). The COV in the horizontal and vertical dimensions (s_{COV} and q_{COV}, respectively) was calculated using the following equations:

$$s_{COV}=\frac{\pi}{V_{body}}\sum_{i=1}^{n}s_i a_i b_i\,\Delta s\,, \quad (5)$$

$$q_{COV}=\frac{\pi}{V_{body}}\sum_{i=1}^{n}q_i a_i b_i\,\Delta s\,. \quad (6)$$

The COM calculation was made by subtracting the mass of tissue occupied by the swim bladder and adding the small contribution made by the oxygen within the swim bladder, which was achieved using the following equations:

$$s_{COM}=\frac{\pi\rho_{tissue}}{M_{body}}\sum_{i=1}^{n}s_i a_i b_i\,\Delta y-\frac{V_{SB}s_{SB}\left(\rho_{SB}-\rho_{tissue}\right)}{M_{body}}\,, \quad (7)$$

$$q_{COM}=\frac{\pi\rho_{tissue}}{M_{body}}\sum_{i=1}^{n}q_i a_i b_i\,\Delta s-\frac{V_{SB}q_{SB}\left(\rho_{SB}-\rho_{tissue}\right)}{M_{body}}\,. \quad (8)$$

The moment of inertia was calculated to estimate the degree of body rotation during exposure to a pressure gradient in our mathematical model (described below). This calculation assumes that the body rotates at the COM, about the vertical (q) axis:

$$I=\frac{\rho\pi}{4}\sum_{i=1}^{n}a_i b_i\left(a_i^2+4\left((q_i-q_{COM})^2+(s_i-s_{COM})^2\right)\right)\Delta s\,. \quad (9)$$

Mathematical modeling

We used a mathematical model to relate our measurements of the morphology and specific gravity of the larval body to the flow signals generated during a feeding strike. Consistent with prior models of suction feeding (Wainwright and Day, 2007), we have restricted our consideration to the flow directly in front of a predator's mouth, where velocities are laminar (Day et al., 2005) and driven by a pressure gradient dp/dx (Muller et al., 1982). We used the results of previous flow visualization studies to describe the flow generated near the mouth of both bluegill (*Lepomis macrochirus*) and largemouth bass (*Micropterus salmoides*) (Higham et al., 2006a; Higham et al., 2006b). We extracted values for flow velocity at a distance of half the maximum gape diameter from the predator's mouth ($U_{1/2\,gape}$) from figures of representative recordings [fig. 5A,B in Higham et al. (Higham et al., 2006b)]. In order to find a continuous expression for the change in velocity over time, we performed a least-squares fit of a cubic smoothing spline (the 'csaps' command in Matlab, using default parameter values) to these measurements of flow velocity (Fig. 4).

We used a previously developed hydrodynamic model to estimate the spatial variation in flow created by these predators (Muller et al., 1982). This approach, which uses inviscid vortex filament theory, was verified with flow visualization measurements (Day et al., 2005). Our implementation of this model neglects the effects of a predator's forward movement in favor of a focus on the hydrodynamics of suction feeding. It predicts spatial variation in flow velocity from measurements of $U_{1/2\,gape}$ with the following equation [based on eqn 34 in Muller et al. (Muller et al., 1982)]:

$$U(x)=\sqrt{8}U_{1/2\,gape}h^3(x^2+h^2)^{-3/2}\,, \quad (10)$$

where h is half the maximum gape diameter. In order to calculate the forces acting on the body of a larval prey, we used this equation to calculate the pressure gradient generated by suction feeding. This was determined with the following simplification of the Navier-Stokes equation (Muller et al., 1982):

$$\frac{dp}{dx}=-\rho_{water}\left(\frac{dU}{dt}+U\frac{dU}{dx}\right)\,. \quad (11)$$

We used a first-order approximation (Wainwright and Day, 2007) of the pressure gradient force ($\mathbf{F}_{pressure}$), which is a vector directed towards decreasing pressure along the gradient. It was calculated using the following equation:

$$\mathbf{F}_{pressure}=-V_{body}\frac{dp}{dx}\,. \quad (12)$$

The pressure gradient force is capable of rotating the body of a larva after swim bladder inflation. An inflated swim bladder creates a separation between the COM and the COV for a larva's body because of the low density of air that it contains (Alexander, 1966). The distance between the COM and the COV (measurement described above) creates a lever arm for torque to be generated about the COM because $\mathbf{F}_{pressure}$ acts at the COV. This torque ($\boldsymbol{\tau}$) may be calculated as the cross-product of the

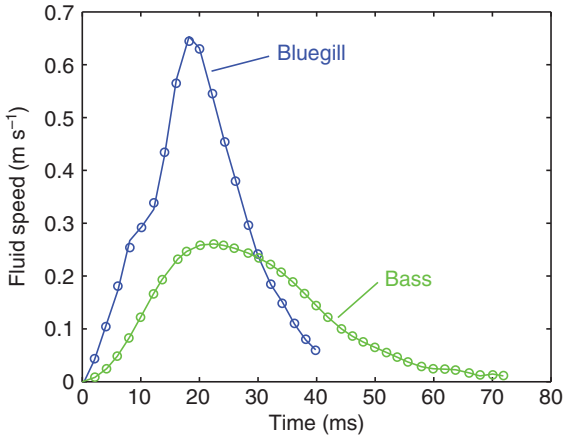

Fig. 4. Fluid velocity from representative suction-feeding strikes of bluegill sunfish (blue) and largemouth bass (green). Measured values (circles) reflect the fluid speeds at a distance of half peak gape from the mouth, as determined by particle image velocimetry in a prior study (Higham et al., 2006b). We fit a smoothing spline (lines) to these values to find a continuous expression from which we mathematically modeled the hydrodynamics of prey capture.

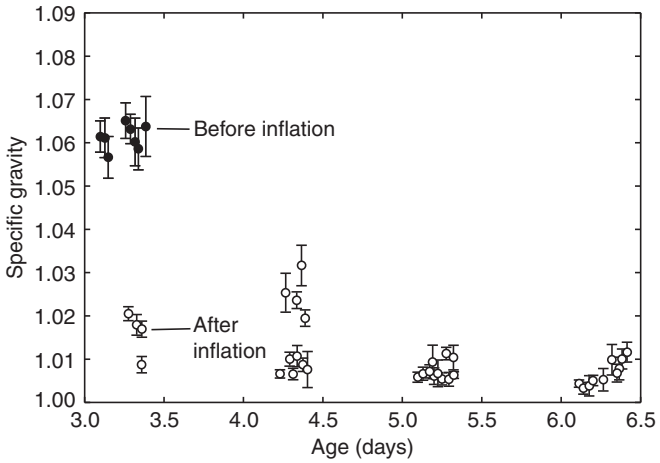

Fig. 5. Specific gravity of the body of zebrafish larvae. The specific gravity (ρ_{body}/ρ_{water}, where ρ_{water}=0.998 g ml^{-1}) was measured from our terminal velocity measurements (Fig. 2) for larvae before (filled circles) and after (open circles) swim bladder inflation. Each point corresponds to a measurement of a single individual and the error bars denote 95% confidence intervals (e.g. Fig. 2E) for each measurement.

pressure force and the position (**D**) of the center of volume with respect to the center of mass:

$$\boldsymbol{\tau} = \mathbf{F}_{pressure} \times \mathbf{D} . \quad (13)$$

We used a numerical solver to calculate the motion of the larval body during suction feeding. The position and velocity of a larva was calculated with an explicit fourth-order Runge-Kutta method (the 'ode45' function in Matlab, with relative and absolute tolerance values of 10^{-6}) that integrated the translational and rotational accelerations of the larval body. The translational acceleration was calculated from our measurement of ρ_{body} under the assumption that $\mathbf{F}_{pressure}$ dominates the fluid forces acting on the body. We evaluated this assumption by calculating the magnitude of drag and the acceleration reaction (described in the Results). The rotational acceleration of the body ($\boldsymbol{\Omega}$) was calculated from our measurements of I (Eqn 9). Therefore, acceleration values were determined using the following equations:

$$\frac{dU_{body}}{dt} = -\frac{1}{\rho_{body}}\frac{dp}{dx} , \quad (14)$$

$$\boldsymbol{\Omega} = \frac{\boldsymbol{\tau}}{I} . \quad (15)$$

For each solution, we determined the velocity of flow from the frame of reference of the larva's body, which we refer to as the relative flow velocity ($U_{relative}$). The relative flow velocity was calculated as the difference in velocity between the water (Eqn 10) and the body ($U_{relative}=U_{water}-U_{body}$).

RESULTS

Specific gravity and morphology of the body

We found that larvae with an inflated swim bladder possessed a lower specific gravity than those without (Fig. 5). Young larvae (<3.5 dpf) without an inflated swim bladder had a nearly 5% greater specific gravity (mean ± s.d., 1.065±0.003, N=8) than larvae with an inflated swim bladder (1.010±0.002, N=35), which was a significant difference (t-test, $P<0.001$). After inflation, neither specific gravity (regression, F=0.0098, P=44.5) nor tissue density (regression, F=3.39, P=0.078) was significantly correlated with age.

Our morphometric analysis showed that swim bladder inflation had a subtle effect on V_{body}. Total V_{body} increased by ~3% (2.97±1.39%) as V_{SB} increased (to 0.00960±0.0026 mm^3, N=23) during inflation. Age did not significantly affect ρ_{tissue} (regression, F=0.414, P=0.526), ρ_{body} (regression, F=0.752, P=0.394; Fig. 6A,B) or I (regression, F=0.242, P=0.627) (N=23). Therefore, our measurements suggest that the observed changes in specific gravity (Fig. 5) may be attributed to swim bladder inflation alone.

Swim bladder inflation also influenced the body position of the COM and COV. Our analysis assumed that density differences among the tissues within the larval body were negligible prior to inflation. As a consequence, the COM was coincident with the COV in these young larvae (Fig. 6C). The low density of gas within the swim bladder caused a slight posterior shift (by 7.44±5.95 µm, N=19) in the position of the COM. We found that the change in body shape to accommodate inflation had a negligible influence on its mass distribution, as measured by I before and after inflation (t-test, d.f.=25, P=0.454). Therefore, a torque about the COM may be generated during suction feeding because $\mathbf{F}_{pressure}$ acts on the COV.

Prey kinematics

Our model predicts that prey capture occurs when larvae are in close proximity to the predator at strike onset. The strike of a bluegill captured larvae at a maximum distance of 10.0 mm from the mouth whereas a bass strike captured prey from up to 14.5 mm away (Fig. 7A). Simulations that considered feeding on larvae at greater distances failed to complete capture within the strike duration (Fig. 4). These maximum capture distances were less than each predator's peak gape (PG) for the strike [PG=11.2 mm for bluegill and PG=29.3 mm for bass; data taken from Higham et al. (Higham et al., 2006b)], with bluegill capable of capturing larvae proportionately further away (90.0% of PG) than bass (49.5% of PG). It should be noted that these calculations neglect any forward motion by the predator or an escape response by the prey.

Our model compared the feeding performance on larvae of different density due to swim bladder inflation. Irrespective of the

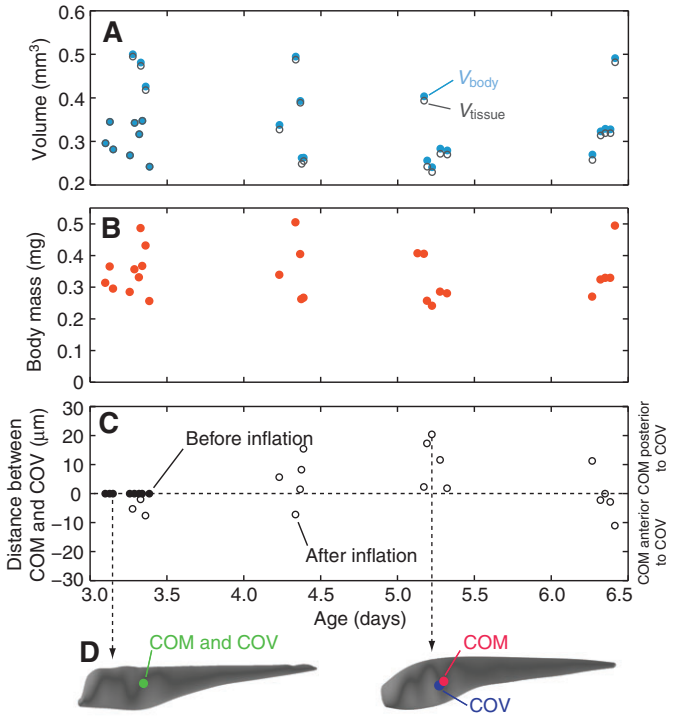

Fig. 6. Body morphology of zebrafish larvae in the first week of growth. (A) Measurements of body volume (V_{body}, blue circles) and tissue volume (V_{tissue}, open circles) from morphometric measurements (as in Fig. 3). (B) Body mass was calculated as the product of specific gravity (Fig. 4), water density and body volume (A). (C,D) The location of the centers of mass (COM) and volume (COV) calculated from reconstructions of larvae. (C) The distance of this separation is plotted with respect to the age of larvae for individuals before (filled circles) and after (open circles) swim bladder inflation. Negative values indicate a COM located anterior to the COV. (D) Representative reconstructions for larvae before (left) and after (right) swim bladder inflation. The COM is coincident with the COV (green circle) prior to inflation, but the COV is anterior to the COM in this larva after inflation.

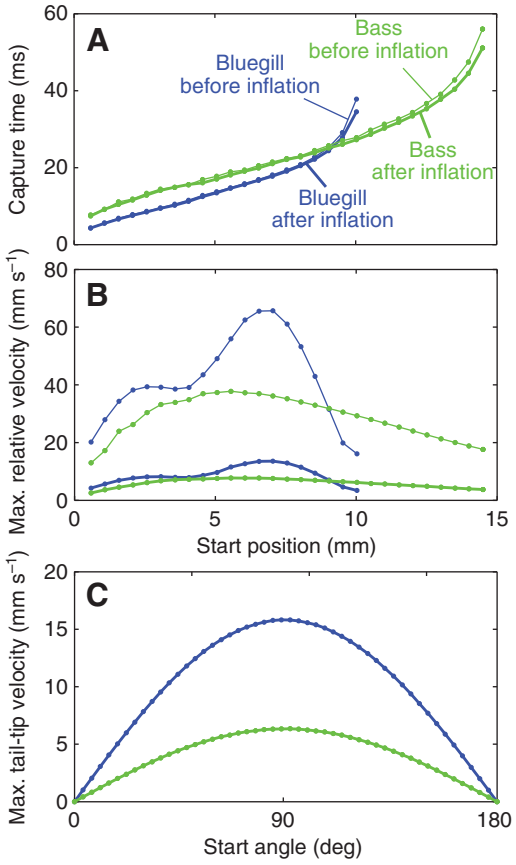

Fig. 7. Predictions of kinematics for feeding performance and flow from numerous simulations. The capture times and maximum fluid velocities experienced by larvae as a function of the larva's initial position and orientation during simulated predator strikes for bluegill (blue) and largemouth bass (green). (A) The time between strike onset and prey capture, as a function of the prey's initial distance from the predator mouth for zebrafish larvae before (thick lines) and after (thin lines) swim bladder inflation. The horizontal ranges for each line indicate the predicted distances in which successful prey capture would occur. The predator suction fields were insufficient to capture prey initially located outside of these ranges. (B) The maximum fluid velocity relative to a larva's body as a function of the larva's initial distance from the predator's mouth. (C) The maximum velocity at a larva's tail tip due only to body rotation as a function of the larva's initial body orientation. For these simulations, larvae were initially located 7.3 mm from the predator's mouth.

starting position of a larva or the predator species, larvae with inflated swim bladders were captured in slightly less time than those with non-inflated swim bladders (Fig. 7A, Fig. 8A). For example, with a starting position of 7.3 mm from the predator mouth, a larva with an inflated swim bladder was captured 0.30 ms earlier than a larva without an inflated swim bladder for bluegill and 0.55 ms earlier for bass (1.60 and 2.40% of the total capture time for larvae with inflated swim bladders, respectively; Fig. 8A).

Simulations considered the flow velocity relative to a larva's body during a strike. This relative flow velocity was very low (<6%) compared to flow velocity in the earthbound frame of reference for all larvae considered. Because of their greater body density, a larva without an inflated swim bladder experiences an approximately fivefold greater relative velocity than a larva with an inflated swim bladder for both predators (Fig. 8C). The maximum relative velocity experienced by a larva during a strike depends on initial position, with a larva located at intermediate distances (~6–7 mm from the predator's mouth) experiencing the highest velocities of 65.7 and 37.8 mm s^{-1} during bluegill and bass strikes, respectively (Fig. 7B). For example, a larva initially located 6 mm in front of a bluegill would enter the predator's mouth after ~20 ms (Fig. 7A), which temporally and spatially coincides with the strike's maximum fluid velocity (Fig. 4).

Our model also evaluated the degree to which the body of a larva rotates during capture by a predator. According to simulations that varied the initial orientation of the body, the separation between the COV and COM created by swim bladder inflation caused noteworthy body rotation. For example, with an initial distance 7.3 mm away from the predator and a body orientation of 45 deg, a larva with an inflated swim bladder rotated almost 1 deg during strikes from either bluegill or bass (Fig. 8D). The tip of the tail is the body position at which the motion induced by this rotation is greatest. The velocity of the tail tip was predicted to be very similar for bass and bluegill strikes until ~14 ms after strike onset (Fig. 8E). After this time, larvae experienced higher tail-tip velocities during strikes by bluegill (18.5 mm s^{-1}) than by bass (5.40 mm s^{-1}) at the time of capture. Tail-tip velocity also depended on the larva's initial body orientation in reference to the predator, with a 90 deg initial orientation at strike onset producing the highest tail-tip with both

bluegill and bass (Fig. 7C). During a bluegill strike, the maximum tail-tip velocity created by rotation exceeded the relative velocity due to translation by a larva with an inflated swim bladder. For example, at the time of capture in bluegill, a larva with an inflated swim bladder oriented at 90 deg experienced a relative velocity and tail-tip velocity of 13.3 and 18.91 mm s^{-1}, respectively (Fig. 8C,E). During the bass strike, the magnitude of relative velocity (7.44 mm s^{-1}) and tail-tip velocity (7.59 mm s^{-1}) at the time of capture were more comparable (Fig. 7B,C).

Our model of larval kinematics assumes that $\mathbf{F}_{pressure}$ dominates the fluid forces that drive a larva's motion towards the predator mouth. To evaluate this assumption, we compared the magnitude of the pressure gradient force (F_P) with other fluid forces under conditions in which those other forces should be maximized. The drag force (F_D) is created by the relative flow velocity in a manner that depends on the Reynolds number (Re) of the larva's body ($Re=LU_{relative}\rho_{water}/\mu$, where L is the larval body length and μ is the dynamic viscosity of water). Our simulations predicted values for relative flow that did not exceed 65 mm s^{-1} for larvae prior to inflation (Fig. 7B). The Re predicted for the most rapid flows ($Re<315$, where $L=4$ mm, $\rho_{water}=996.1$ kg m^{-3} and $\mu=8.23\times10^{-4}$ Pa s) did not exceed the upper limit of the viscous-dominated regime (McHenry and Lauder, 2005). Therefore, drag may be calculated using the following equation (Batchelor, 1967):

$$F_D = C_{visc} L \mu U_{relative}, \quad (16)$$

where C_{visc} is the viscous drag coefficient [$C_{visc}=0.64$ for a zebrafish larva parallel to flow (McHenry and Lauder, 2006)]. Using the same parameter values as the Re calculation, F_D (<0.14 μN) was found to be about 15 times less than F_P (2.12 μN, calculated using Eqn 12 with $V_{body}=3.03\times10^{-10}$ m^3 and $dp/dx=-7.02\times10^3$ kg m^{-2} s^{-2}) and is anticipated to be substantially less under most circumstances. Furthermore, when the swim bladder inflates and causes the relative velocity to decrease to one-fifth of the pre-inflation levels, F_D decreases proportionately. As a consequence, F_P is predicted to be more than 75 times greater in magnitude than F_D in a larva with an inflated swim bladder.

The acceleration reaction force (F_{AR}) arises from the acceleration of water around the fish's body. The acceleration reaction force may be calculated using the following equation (Denny, 1988):

$$F_{AR} = A\rho_{water} V_{body} a, \quad (17)$$

where a is the relative acceleration of the body and A is the added mass coefficient. We assumed that the body of a larval fish has the same added mass coefficient as an 1:6 ellipsoid [$A=0.045$ (McHenry and Lauder, 2005)]. The F_P was found to be at least 19 times greater than F_{AR} (<0.11 μN, where $V_{body}=3.03\times10^{-10}$ m^3 and $a=6.0$ m s^{-2}) in larvae before inflation and nearly 100 times greater in larvae after inflation. Therefore, neglecting F_D and F_{AR} provides a reasonable first-order approximation of the force acting to accelerate the body, especially for larvae with an inflated swim bladder. Inclusion of these forces would provide a very slight reduction in the relative velocity predicted.

DISCUSSION

This study demonstrates how the ability of a prey fish to sense a predator depends on the specific gravity of the prey's body. Using a novel technique, we have demonstrated that the specific gravity of a zebrafish larva's body decreases by 5% when its swim bladder inflates (Fig. 5). According to a hydrodynamic model that we developed, this subtle change is predicted to cause a dramatic 80% reduction in the flow velocity around the prey when it is attacked by a predator (Fig. 7B). Although these differences in specific gravity are predicted to have a negligible effect on the period of time available for a larva to escape (Fig. 7A), the reduction in flow velocity presents a substantial attenuation in the stimulus available to the lateral line system. Therefore, small changes in specific gravity may greatly alter the ability of a prey fish to evade capture.

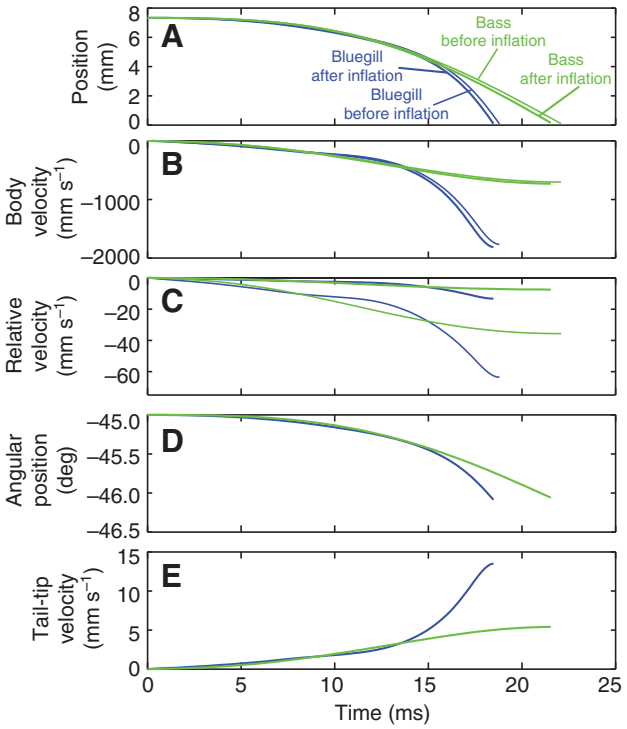

Fig. 8. Predicted kinematics and flow of zebrafish larvae during a predator's strike. Representative simulations are shown for larvae before (thin lines) and after (thick lines) swim bladder inflation for suction-feeding strikes of bluegill (blue lines) and largemouth bass (green lines). (A) The position of a larva's body, measured by the distance from the predator's mouth from a starting position of 7.3 mm. (B) The velocity of the prey's body in the earthbound frame of reference as it moves toward the predator's mouth during a strike and (C) the flow velocity in the prey's frame of reference (i.e. relative flow velocity). In B and C, negative velocities reflect movement toward the predator. (D) The rotation of the larval body during a strike for an initial angle of 45 deg. Larvae without an inflated swim bladder exhibited no rotation because the COV is coincident with the COM. (E) The fluid speed at the tail tip resulting from the body rotation in panel (D).

Changes in specific gravity with growth

The specific gravity of a fish's body changes throughout growth (Lindsey et al., 2010). In many species, a hatchling larva carries yolk that is mostly composed of proteins and lipids, which are quickly metabolized as the larva begins to forage. Although yolk composition varies greatly among species, its density generally decreases with age (Heming and Buddington, 1988; Wiegand, 1996). Zebrafish larvae possess a small yolk compared with that of other fish [e.g. salmonids (Hale, 1999)] and we found that digesting this volume did not have a significant change on the density of the body in the first week of growth (Fig. 5). In subsequent growth, the density of a fish's body increases more gradually, primarily owing to the calcification of the skeleton (Alexander, 1966; Heming and Buddington, 1988). Although changes in zebrafish body density throughout ontogeny have been investigated elsewhere (Lindsey et al., 2010), the present study is the

first to provide highly precise measurements of body density over the short and crucial growth stage when the swim bladder inflates.

The swim bladder provides a fish with the ability to alter the specific gravity of its body. As our measurements demonstrate (Fig. 5), swim bladder inflation decreases the specific gravity of the body in zebrafish by nearly 5% (from 1.063 to 1.011) and thereby causes the body to approach neutral buoyancy. This change is correlated with an increase in the frequency of spontaneous swimming as a larva begins to forage for food (Robertson et al., 2007). The approach towards neutral buoyancy has the benefit of reducing the demand to generate propulsive forces to overcome gravity. Furthermore, a fish may regulate specific gravity against changes in hydrostatic pressure (Alexander, 1993) and tissue density (Alexander, 1966) with minute alterations in the volume of air within the swim bladder.

Prey-capture kinematics

Our results suggest that swim bladder inflation has a minor effect on the time it takes for a predator to capture a passive prey. For example, a larva positioned 7 mm from the mouth of a bass was captured in 21.0 ms if its swim bladder was inflated or 21.5 ms if not inflated (Fig. 7A). This small difference (2.4%) was due to an increase in the pressure gradient force (Eqn 12) caused by a slight rise in body volume from inflation (Fig. 6A). This slight difference demonstrates that larvae have about the same time to escape, regardless of their specific gravity. However, as discussed below, a difference in specific gravity can have a large effect on the ability to sense the strike with the lateral line system. Whether a larva can effectively evade the strike will depend on the rate and direction of the escape response triggered by this stimulus, which we did not consider in the present study.

Our measurements of body volume and density provide precise measurements that can be incorporated into models of prey capture. Prior modeling has employed rough approximations for these parameters. For example, the body of a prey has been modeled as a sphere with neutral buoyancy (Wainwright and Day, 2007; Van Wassenbergh and Aerts, 2009; Skorczewski et al., 2010). Although our measurements offer an improvement in precision, our simulation results suggest that model predictions are not highly sensitive to these parameters. Therefore, the approximations made in earlier studies were sufficient to model the major dynamics of prey capture.

Lateral line function

We found that changes in specific gravity that accompany swim bladder inflation affect lateral line function. The superficial neuromasts of the lateral line system of larval fish are sensitive to the flow velocity relative to the body (Fig. 1) (Windsor and McHenry, 2009; van Netten, 2006). According to our model, swim bladder inflation causes a nearly 80% reduction in maximum relative velocity, irrespective of the distance between the predator and prey at the start of a strike (Fig. 7B). Swim bladder inflation reduces a larva's specific gravity, which causes it to move more closely in unison with the surrounding water during a strike. This reduces the flow velocity relative to the larva and creates a weaker signal for the superficial neuromasts of the lateral line system.

Swim bladder inflation is predicted to cause the body to rotate during a feeding strike. The body rotates with an acceleration that is proportional to the distance between the COM and COV and depends on body orientation with respect to flow velocity (Eqns 13, 15). Our simulations predict that rotation can create a flow stimulus that is comparable to that generated by body translation in larvae with inflated swim bladders. For example, the velocity experienced by the larval tail-tip due to rotation exceeded relative velocity for a starting orientation of 90 deg during a bluegill strike (Fig. 7B,C). This result is consistent with the recent finding that zebrafish larvae in a pressure gradient are more likely to respond to flow velocity that is directed normal to the longitudinal axis of the body than when velocity is parallel (Feitl et al., 2010). Therefore, the reduction in a flow stimulus caused by lower specific gravity may be countered by enhanced body rotation when the swim bladder inflates.

It is only a slight deviation of the specific gravity of a body from unity (Fig. 5) that creates the relative flow that may be detected by the lateral line system. As a consequence, the relative flow velocity predicted by our model was very low (<6%) compared with the flow velocity in the earthbound frame of reference. This illustrates the fundamental importance of the frame of reference to the signals detected by a prey fish. Despite the relatively slight magnitude to the flow stimulus, larval zebrafish are highly adept at sensing the flow of a predator's strike with the lateral line system (McHenry et al., 2009).

The hydrodynamics of larval fish considered in the present study may occur in fish of any size or stage of growth. For example, an adult fish that is swept downstream in a current also experiences a pressure gradient of flow. As in larval prey, the size and mass of the body of an adult fish will affect the relative flow velocity and, hence, the signal detected by the superficial neuromasts. However, an adult may extract additional information from this stimulus owing to differences in their lateral line system. Most notable among these differences are the canal neuromasts, which are present in adults but not larvae. Like a superficial neuromast, a canal neuromast generates a neurobiological signal from the flow-induced deflections of its cupula (Dijkgraaf, 1963). However, a canal neuromast resides within a channel beneath the scales. Flow is induced through the channel when a pressure difference is created at the pores that open the channel to the surface of the skin. As a consequence, a canal neuromast functions as a pressure gradient sensor that does not require a difference in velocity between the body and water to detect a signal (van Netten, 2006). Therefore, despite similarities in the hydrodynamics of adult and larval fish, the lateral line system may detect different signals at these two stages of growth.

The lateral line system is capable of playing a role on both sides of a predator–prey interaction between fish. In the dark, adult fish may use their canal neuromasts to localize prey from spatial patterns in pressure gradients created by swimming (Coombs and Conley, 1997). The relatively large size of the predator's body provides the opportunity to use this array of neuromasts to triangulate the direction and proximity of the prey. The capacity of larval prey to sense the predator appears to be more limited. The lateral line system can initiate an escape response as a predator strikes (McHenry et al., 2009), but the small size of their body and the slow motion of the predator probably restricts their ability to sense a predator with their lateral line prior to the strike.

In summary, our results suggest that subtle changes in the specific gravity of a prey fish can greatly affect the ability to sense the flow of a suction-feeding predator. Swim bladder inflation decreases specific gravity by ~5% (Fig. 5A), which creates an 80% reduction in the relative flow velocity that may be sensed by the lateral line system (Fig. 7B). This attenuation in the flow stimulus may be countered by body rotation in a larva with an inflated swim bladder (Fig. 7C). Furthermore, capture time was virtually unaltered by inflation (Fig. 7A). Therefore, the specific gravity of a prey is crucial to its ability to sense a predator but it does not affect the brief duration available to evade the strike with an escape response.

ACKNOWLEDGEMENTS

This research project was supported by the NSF (IOS-0952344 and IOS-0723288).

REFERENCES

Alexander, R. M. (1966). Physical aspects of swim bladder function. *Biol. Rev. Camb. Philos. Soc.* **41**, 141-176.
Alexander, R. M. (1993). Buoyancy. In *The Physiology of Fishes* (ed. D. H. Evans), pp. 75-97. Boca Raton, FL: CRC Press.
Batchelor, G. K. (1967). *An Introduction to Fluid Dynamics*. New York: Cambridge University Press.
Brand, M., Granato, M. and Nuesslein-Volhard, C. (2002). Keeping and raising zebrafish. In *Zebrafish* (ed. C. Nusslein-Volhard and R. Dahm), pp. 7-38. Oxford: Oxford University Press.
Coombs, S. H. (1981). A density-gradient column for determining the specific gravity of fish eggs, with particular reference to eggs of the mackerel *Scomber scombrus*. *Mar. Biol.* **63**, 101-106.
Coombs, S. and Conley, R. A. (1997). Dipole source localization by mottled sculpin. I. Approach strategies. *J. Comp. Physiol. A* **180**, 387-399.
Day, S. W., Higham, T. E., Cheer, A. Y. and Wainwright, P. C. (2005). Spatial and temporal patterns of water flow generated by suction-feeding bluegill sunfish *Lepomis macrochirus* resolved by particle image velocimetry. *J. Exp. Biol.* **208**, 2661-2671.
Denny, M. W. (1988). *Biology and the Mechanics of the Wave-Swept Environment.* Princeton, NJ: Princeton University Press.
Dijkgraaf, S. (1963). The functioning and significance of the lateral line organs. *Biol. Rev.* **38**, 51-105.
Eaton, R. C., Bombardieri, R. A. and Meyer, D. L. (1977). Mauthner-initiated startle response in teleost fish. *J. Exp. Biol.* **66**, 65-81.
Feitl, K. E., Ngo, V. and McHenry, M. J. (2010). Swimming reduces the responsiveness of fish to a flow stimulus. *J. Exp. Biol.* **213**, 3131-3137.
Ferry-Graham, L. A. and Lauder, G. V. (2001). Aquatic prey capture in ray-finned fishes: a century of progress and new directions. *J. Morphol.* **248**, 99-119.
Hale, M. E. (1999). Locomotor mechanics during early life history: effects of size and ontogeny on fast-start performance of salmonid fishes. *J. Exp. Biol.* **202**, 1465-1479.
Heming, T. A. and Buddington, R. K. (1988). Yolk sac absorption in embryonic and larval fishes. In *Fish Physiology* (ed. W. A. Hoar and D. J. Randall), pp. 407-446. London: Academic Press.
Higham, T. E., Day, S. W. and Wainwright, P. C. (2006a). The pressures of suction feeding: the relation between buccal pressure and induced fluid speed in centrarchid fishes. *J. Exp. Biol.* **209**, 3281-3287.
Higham, T. E., Day, S. W. and Wainwright, P. C. (2006b). Multidimensional analysis of suction feeding performance in fishes: fluid speed, acceleration, strike accuracy and the ingested volume of water. *J. Exp. Biol.* **209**, 2713-2725.
Holzman, R. and Wainwright, P. C. (2009). How to surprise a copepod: Strike kinematics reduce hydrodynamic disturbance and increase stealth of suction-feeding fish. *Limnol. Oceanogr.* **54**, 2201-2212.
Holzman, R., Day, S. W. and Wainwright, P. C. (2007). Timing is everything: coordination of strike kinematics affects the force exerted by suction feeding fish on attached prey. *J. Exp. Biol.* **210**, 3328-3336.
Juanes, F., Buckel, J. A., Scharf, F. S. and Hart, P. J. B. (2002). Feeding ecology of piscivorous fishes. In *The Handbook of Fish Biology and Fisheries: the Biology, Conservation, and Management of Exploited Species* (ed. P. J. B. Hart and J. D. Reynolds), pp. 267-283. London: Blackwell Scientific.
Lauder, G. V. (1980). The suction feeding mechanism in sunfishes (*Lepomis*) – an experimental analysis. *J. Exp. Biol.* **88**, 49-72.
Lauder, G. V. and Clark, B. D. (1984). Water-flow patterns during prey capture by teleost fishes. *J. Exp. Biol.* **113**, 143-150.
Lindsey, B. W., Smith, F. M. and Croll, R. P. (2010). From inflation to flotation: contribution of the swimbladder to whole-body density and swimming depth during development of the zebrafish (*Danio rerio*). *Zebrafish* **7**, 85-96.
McHenry, M. J. and Lauder, G. V. (2005). The mechanical scaling of coasting in zebrafish (*Danio rerio*). *J. Exp. Biol.* **208**, 2289-2301.
McHenry, M. J. and Lauder, G. V. (2006). Ontogeny of form and function: Locomotor morphology and drag in zebrafish (*Danio rerio*). *J. Morphol.* **267**, 1099-1109.
McHenry, M. J., Feitl, K. E., Strother, J. A. and Van Trump, W. J. (2009). Larval zebrafish rapidly sense the water flow of a predator's strike. *Biol. Lett.* **5**, 477-479.
Muller, M., Osse, J. W. M. and Vergagen, J. H. G. (1982). A quantitative hydrodynamical model of suction feeding in fish. *J. Theor. Biol.* **95**, 45-79.
Robertson, G. N., McGee, C. A. S., Dumbarton, T. C., Croll, R. P. and Smith, F. M. (2007). Development of the swimbladder and its innervation in the zebrafish, *Danio rerio*. *J. Morphol.* **268**, 967-985.
Robertson, G. N., Lindsey, B. W., Dumbarton, T. C., Croll, R. P. and Smith, F. M. (2008). The contribution of the swimbladder to buoyancy in the adult Zebrafish (*Danio rerio*): a morphometric analysis. *J. Morphol.* **269**, 666-673.
Scholander, P. F., Claff, C. L., Teng, C. T. and Walters, V. (1951). Nitrogen tension in the swimbladder of marine fishes in relation to the depth. *Biol. Bull.* **101**, 178-193.
Skorczewski, T., Cheer, A., Cheung, S. and Wainwright, P. C. (2010). Use of computational fluid dynamics to study forces exerted on prey by aquatic suction feeders. *J. R. Soc. Interface* **7**, 475-484.
Stenevik, E. K., Sundby, S. and Agnalt, A. L. (2008). Buoyancy and vertical distribution of Norwegian coastal cod (*Gadus morhua*) eggs from different areas along the coast. *ICES J. Mar. Sci.* **65**, 1198-1202.
Van Leeuwen, J. L. and Muller, M. (1984). Optimum sucking techniques for predatory fish. *Trans. Zool. Soc. Lond.* **37**, 137-170.
van Netten, S. M. (2006). Hydrodynamic detection by cupulae in a lateral line canal: functional relations between physics and physiology. *Biol. Cybern.* **94**, 67-85.
Van Wassenbergh, S. and Aerts, P. (2009). Aquatic suction feeding dynamics: insights from computational modelling. *J. R. Soc. Interface* **6**, 149-158.
Wainwright, P. C. and Day, S. W. (2007). The forces exerted by aquatic suction feeders on their prey. *J. R. Soc. Interface* **4**, 553-560.
Wainwright, P., Carroll, A. M., Collar, D. C., Day, S. W., Higham, T. E. and Holzman, R. A. (2007). Suction feeding mechanics, performance, and diversity in fishes. *Integr. Comp. Biol.* **47**, 96-106.
Westerfield, M. (1993). *The Zebrafish Book: a Guide for the Laboratory use of Zebrafish (Brachydanio rerio).* Eugene, OR: University of Oregon Press.
Wiegand, M. D. (1996). Composition, accumulation and utilization of yolk lipids in teleost fish. *Rev. Fish Biol. Fish.* **6**, 259-286.
Windsor, S. P. and McHenry, M. J. (2009). The influence of viscous hydrodynamics on the fish lateral-line system. *Integr. Comp. Biol.* **49**, 691-701.